HHS Public Access

Author manuscript

Nat Struct Mol Biol. Author manuscript; available in PMC 2017 January 11.

Published in final edited form as:

Nat Struct Mol Biol. 2016 August ; 23(8): 752–754. doi:10.1038/nsmb.3258.

Structure of NS3 helicase from Zika virus

Rinku Jain[1], **Javier Coloma**[1], **Adolfo García-Sastre**[2,3,4], and **Aneel K. Aggarwal**[1,¶]

[1]Department of Structural & Chemical Biology, Icahn School of Medicine at Mount Sinai, New York, New York, USA

[2]Department of Microbiology, Icahn School of Medicine at Mount Sinai, New York, New York, USA

[3]Global Health and Emerging Pathogens Institute, Icahn School of Medicine at Mount Sinai, New York, New York, USA

[4]Department of Medicine, Division of Infectious Diseases, Icahn School of Medicine at Mount Sinai, New York, New York, USA

Abstract

The Zika virus has emerged as a pathogen of major health concern. We present a high-resolution (1.62Å) crystal structure of the RNA helicase from the French Polynesia strain. The structure is similar to that of the RNA helicase from Dengue virus, with variability in the conformations of loops typically involved in ATP and RNA binding. We identify druggable “hotspots” that are well-suited for *in-silico* and/or fragment-based high throughput drug discovery.

The Zika virus (ZIKV) has emerged as a major health hazard over the past year, linked to microcephaly in newborn infants and the Guillan-Barré syndrome in adults [1]. ZIKV belongs to the same *Flavivirus* genus as other mosquito-borne human pathogens, such as dengue virus (DENV1-4), tick-borne encephalitis virus (TBEV), Japanese encephalitis virus (JEV), yellow fever virus (YFV), West Nile virus (WNV), Murray Valley encephalitis virus (MVEV) and Kokobera virus (KOKV), among others. The public health emergency posed by ZIKV has invigorated efforts to develop a vaccine, as well as measures to eradicate the *Aedes* mosquito vectors. In addition to these measures, it is equally important to develop antivirals based on the targeting of enzymatic activities central to the life cycle and survival of ZIKV. One such enzymatic activity is encoded by the C-terminal region of the non structural protein NS3 in flaviviruses, namely an RNA helicase (NS3-Hel) involved in genome replication and RNA synthesis [2, 3]. NS3-Hel belongs to the superfamily 2 (SF2) of helicases [4] and its inactivation in DENV2 renders the virus incapable of replicating

¶Correspondence: aneel.aggarwal@mssm.edu.

Accession codes: Atomic coordinates and structure factors have been deposited in the Protein Data Bank under accession codes 5JRZ.

Author contributions

R.J, A.K.A and A.G.S designed the experiments; R.J performed protein expression and purification, and crystallization. R.J and J.C performed crystallography. A.K.A, R.J and J.C wrote the paper. All authors reviewed the manuscript.

Competing financial interests

The authors declare that they have no competing financial interests

properly [5]. To help guide the discovery of antiviral compounds against ZIKV, we present here a high-resolution (1.62Å) crystal structure of NS3-Hel from the French Polynesia strain of the virus.

We expressed and purified ZIKV NS3-Hel (residues 171–617) of the H/PF/2013 strain as a soluble protein from *E. coli* (Online Methods). The structure was determined by molecular replacement, and refined to a resolution of 1.62 Å with R_{work} and R_{free} values of 16.1 % and 19.3 %, respectively (Supplementary Table 1). The refined model consists of one NS3-Hel molecule (residues 175–617), one pyrophosphate and six acetate ions, and 552 solvent molecules.

ZIKV NS3-Hel is composed of three domains of roughly similar size (Fig. 1a). Domains 1 and 2 (residues 182:327 and 328:480 respectively) comprise the tandem α/β RecA-like folds characteristic of SF1 and SF2 helicases [4]. Domain 1 contains the classical motifs I/P-loop (or Walker A), Ia, II (or Walker B), and III, whereas domain 2 contains the motifs IV, IVa, V, and VI (Supplementary Fig. 1). These helicase motifs are typically associated with ATP binding and/or hydrolysis (motifs I, II, and VI), interdomain communication, and RNA binding (motifs Ia, IV, and V) and line a cleft at the interface of domains 1 and 2 (Fig. 1a, Supplementary Fig. 1). As with the closely related DENV4 helicase (Fig. 1a), for which there are structures in different ligand bound states [6], ATP is expected to bind to the "bottom" side of the cleft between domain 1 and 2, while the RNA would be accommodated in a tunnel that separates domains 1 and 2 from domain 3. Curiously, we observe electron density about the size of a pyrophosphate near the P-loop in the ATP binding cleft (Fig. 2a). Guided by its shape and size, we modeled this extra density both as glycerol (present in the purification buffer and cryoprotectant) and pyrophosphate, but the best fit is obtained with a pyrophosphate (Supplementary Fig. 2a), which may have been acquired during expression of the protein in *E. coli*[7]. The putative pyrophosphate is in a similar position as the β- and γ-phosphates of AMPNP in the DENV4 NS3-Hel/AMPNP structure [6] (Supplementary Fig. 2b), with the capacity to make hydrogen bonds with the main chain and side chains atoms of the conserved P-loop (Fig. 2a). It is not uncommon for an NTPase to co-purify with a pyrophosphate, as for example, in structures of KOKV NS3-Hel[8] and *H.pylori* GTP cyclohydrolase[9]. A β-hairpin extends from domain 2 and interacts with domain 3 and has been proposed to act as a "wedge" to help separate the RNA strands of dsRNA for the unwinding reaction (Fig. 1a)[6]. Interestingly, the β-hairpin in our structure (residues 431–444) is slightly smaller than in the DENV4 helicase (430–445) (Fig. 2b) and may alter the kinetics of the RNA unwinding reaction. Domain 3 is predominantly α-helical. In addition to contacts with RNA it has also been implicated in interactions with the RNA-dependent RNA polymerase NS5 in other flaviviruses [10].

Overall, all three domains superimpose very well on equivalent domains in other flaviviruses (Supplementary Fig. 3a). ZIKV domains 1, 2, and 3 superimpose with r.m.s. deviations of 0.60 Å, 0.31 Å and 0.40 Å, respectively on the equivalent domains of DENV4. However, there are some qualitative differences in the electrostatic surface of ZIKV NS3-Hel when compared to other flaviviruses, including an RNA binding groove that is somewhat less basic (Supplementary Fig. 4). Additional comparison between ZIKV and the other flavivirus NS3-Hel structures highlights flexibility in the relative orientation of domains 1 and 2 (Fig.

2b), and in the conformation of loops implicated in ATP and RNA binding (Supplementary Figs. 3b and 3c). Compared to the apo DENV4 helicase, domain 2 of ZIKV helicase is rotated away from domain 1 by ~13°, leading to a wider ATP binding cleft (Fig. 2b). Interestingly, apo WNV, YFV, KOKV, and JEV also adopt the ZIKV-like partially open conformation [11, 12], whereas DENV2 and MVEV assume the DENV4-like closed conformation [13, 14]. The P-loop (residues 196–203) and the RNA binding loop (residues 244–255) in our structure adopt conformations similar to that when DENV4 NS3-Hel binds to ATP and ssRNA - rather than the apoenzyme [6]. The P-loops in other flavivirus apo structures also assume conformations similar to that in ZIKV (Supplementary Fig. 3b), whereas their RNA binding loops are partially disordered (Supplementary Fig. 3c). Altogether, the P-loop and the RNA-binding loop are the most flexible segments in NS3-Hel structures and intermittently sample conformations of the ligand bound state [15].

Is the ZIKV NS3-Hel a druggable target? We used the program FTMap to derive druggable "hotspots" on the ZIKV helicase surface [16]. FTMap maps clusters of small organic molecules on a protein surface as putative drug/ligand binding sites. The two most prominent sites on the ZIKV NS3-Hel are between domains 1 and 2 (site 1) and at the confluence of domains 1 and 3 (site 2) (Fig. 3). Site 1 is close to the extra "pyrophosphate" density in our structure, while site 2 is within the RNA binding groove, close to the putative 3' end of bound RNA. Both pockets possess polar and hydrophobic characteristics and appear well-suited for *in-silico* high throughput screening with drug-like molecules and/or fragment based screening [17, 18]. Also, the close proximity of the two pockets may lend to the design of inhibitors that can span both sites. Several inhibitors have been reported for DENV helicase [19]. It will be interesting to see if they bind the ZIKV helicase and mitigate the ability of the virus to replicate.

In conclusion, we report here a high resolution crystal structure of ZIKV RNA helicase that will aid in the discovery of antiviral compounds against this emerging, pernicious pathogen.

Note added in proof: While this paper was under review, the structure of ZIKV NS3-Hel was published at 1.8 Å resolution[20], showing similar structure to that described here but without a pyrophosphate.

Online Methods

Purification, crystallization and structure determination

ZIKV NS3-Hel (171–617) from the H/PF/2013 strain was expressed and purified from *Escherichia coli* strain B834(DE3) with a N-terminal His_6-SUMO tag. Cell pellets containing the recombinant protein were resuspended in buffer containing 50 % B-PER (Thermo Scientific), 25 mM Tris, pH 8.0, 500 mM NaCl, 10 % sucrose, and 5 mM 2-mercaptoethanol (BME). Cells were lysed by sonication and the filtered lysate was loaded on a 5 mL Ni-NTA column (Qiagen). Protein bound to the Ni-NTA column was eluted with buffer containing 50 mM Tris-HCl, pH 8.0, 500 mM NaCl, 5 % glycerol, 5 mM BME and 300 mM imidazole. Eluted protein was dialyzed into buffer containing 50 mM Tris, pH 8.0, 150 mM NaCl, 1 mM DTT and 0.01 % IGEPAL CA-630. The His_6-SUMO tag was cleaved with Ulp protease and the protein re-loaded on the Ni-NTA column to remove the cleaved

His_6-SUMO tag and any uncleaved protein. The cleaved protein was purified further by ion exchange chromatography on an anion exchange column or by size exclusion chromatography on a SD75 column (GE Healthcare Life Sciences). Before crystallization, the protein was concentrated to 10 mg/ml in buffer containing 25 mM Tris, pH 8.0, 100 mM NaCl, and 2 mM TCEP.

Initial screens were set up with the Oryx robot at 4 °C. Thin plate like crystals were obtained in conditions containing PEG8K, MOPS buffer and 200 mM magnesium acetate from the Protein Complex suite (Qiagen). Crystals were optimized by varying the concentration of PEG 8K and microseeding. Stock solutions for crystal optimization consisted of 50 % w/v PEG 8K (Sigma-Aldrich), 0.1 M MOPS (NaOH), pH 7.0, and 2 M magnesium acetate (Fluka). Crystals used for data collection grew out of drops containing 4–8 % PEG 8K, 0.1 M MOPS, pH 7.0, 100 mM magnesium acetate.

For data collection, crystals were cryoprotected by quick dipping in mother liquor containing 30 % glycerol alone, or in a mixture of 9 % sucrose, 2 % glucose, 8 % glycerol and 8 % ethylene glycol and flash-cooled in liquid nitrogen. Diffraction data was collected at the Advanced Photon Source (beamline 24-ID-E) under cryogenic conditions at a wavelength of 0.97918 Å, and indexed with HKL2000 [21].

The ZIKV NS3-Hel structure was solved by molecular replacement using the Auto-Rickshaw web server (http://webapps.embl-hamburg.de/cgi-bin/Auto-Rick/arinitAR1.cgi)[22]. Model obtained from the Auto-Rickshaw pipeline was improved by iterative manual building and refinement with Coot [23] and Phenix [24] respectively. After the protein chain was built, difference electron density (greater than 3σ) was visible near the P-loop (Fig. 2a and Supplementary Fig. 2), indicating the presence of a ligand. Automated ligand identification with Phenix suggested the presence of either bulky amino acid (Arg, Glu, Lys, Trp and Met), nucleotides with the phosphate moiety in the difference density, pyrophosphate, or glycerol. Visual inspection of the fit of these putative ligands into the difference density, residual density after refinement with Phenix, and their interactions with the neighboring protein residues suggested that the density was best described as a pyrophosphate. The pyrophosphate moiety is engaged in putative hydrogen bonding interactions with the P-loop residues, Gly197, Gly 199 and Lys200, as well as with the side chain of Arg462.

The final model was refined to 1.62 Å and has good stereochemistry with 98 % of the residues in the most favored regions of the Ramachandran plot and 0.2 % in the disallowed regions. Figures were prepared using PyMol (https://www.pymol.org/). Qualitative surface electrostatic potential for the Flavivirus NS3-helicase domains (Supplementary Fig. 4) were computed with PyMol. The potential range was set the same for all the structures, with positive potential shown in blue and negative potential in red.

Mapping druggable hotspots with FTmap

The FTmap server (http://ftmap.bu.edu) was used to identify hot spots of ZIKV NS3-Hel and determine its druggability. These are cavities on the protein surface that represent potential ligand binding sites. The program was run with default parameters. 11 hot spots were predicted and the number of probe clusters at these sites were 28, 26, 11, 8, 5, 4, 4 3, 2,

2, and 2 from the highest to the lowest ranked hot spot. These hot spots coalesce into two broad and contiguous sites (sites 1 and 2, see Fig. 3) in the vicinity of the RNA binding groove and ATP binding cleft.

Supplementary Material

Refer to Web version on PubMed Central for supplementary material.

Acknowledgments

We thank K. Rajashankar and the staff at NECAT-24ID (APS) for facilitating data collection. These studies were partly funded by a supplement to the NIAID NIH grant U19AI118610 (to AG-S).

References

1. Petersen LR, Jamieson DJ, Powers AM, Honein MA. N Engl J Med. 2016; 374:1552–1563. [PubMed: 27028561]
2. Frick DN, Lam AM. Curr Pharm Des. 2006; 12:1315–1338. [PubMed: 16611118]
3. Luo D, Vasudevan SG, Lescar J. Antiviral Res. 2015; 118:148–158. [PubMed: 25842996]
4. Singleton MR, Dillingham MS, Wigley DB. Annu Rev Biochem. 2007; 76:23–50. [PubMed: 17506634]
5. Matusan AE, Pryor MJ, Davidson AD, Wright PJ. J Virol. 2001; 75:9633–9643. [PubMed: 11559795]
6. Luo D, et al. EMBO J. 2008; 27:3209–3219. [PubMed: 19008861]
7. Kukko E, Heinonen J. Eur J Biochem. 1982; 127:347–349. [PubMed: 6291941]
8. Speroni S, et al. Proteins. 2008; 70:1120–1123. [PubMed: 18004778]
9. Yadav S, Karthikeyan S. J Struct Biol. 2015; 192:100–115. [PubMed: 26272484]
10. Tay MY, et al. J Biol Chem. 2015; 290:2379–2394. [PubMed: 25488659]
11. Wu J, Bera AK, Kuhn RJ, Smith JL. J Virol. 2005; 79:10268–10277. [PubMed: 16051820]
12. Mastrangelo E, et al. J Mol Biol. 2007; 372:444–455. [PubMed: 17658551]
13. Mancini EJ, et al. Protein Sci. 2007; 16:2294–2300. [PubMed: 17893366]
14. Xu T, et al. J Virol. 2005; 79:10278–10288. [PubMed: 16051821]
15. Boehr DD, Nussinov R, Wright PE. Nat Chem Biol. 2009; 5:789–796. [PubMed: 19841628]
16. Kozakov D, et al. Nat Protoc. 2015; 10:733–755. [PubMed: 25855957]
17. Rees DC, Congreve M, Murray CW, Carr R. Nat Rev Drug Discov. 2004; 3:660–672. [PubMed: 15286733]
18. Shoichet BK. Nature. 2004; 432:862–865. [PubMed: 15602552]
19. Sweeney NL, et al. ACS Infect Dis. 2015; 1:140–148. [PubMed: 26029739]
20. Tian H, et al. Protein Cell. 2016; 7:450–454. [PubMed: 27172988]
21. Otwinowski Z, Minor W. Methods Enzymol. 1997; 276:307–326. [PubMed: 27754618]
22. Panjikar S, Parthasarathy V, Lamzin VS, Weiss MS, Tucker PA. Acta Crystallogr D Biol Crystallogr. 2005; 61:449–457. [PubMed: 15805600]
23. Emsley P, Cowtan K. Acta Crystallogr D Biol Crystallogr. 2004; 60:2126–2132. [PubMed: 15572765]
24. Adams PD, et al. Acta Crystallogr D Biol Crystallogr. 2010; 66:213–221. [PubMed: 20124702]

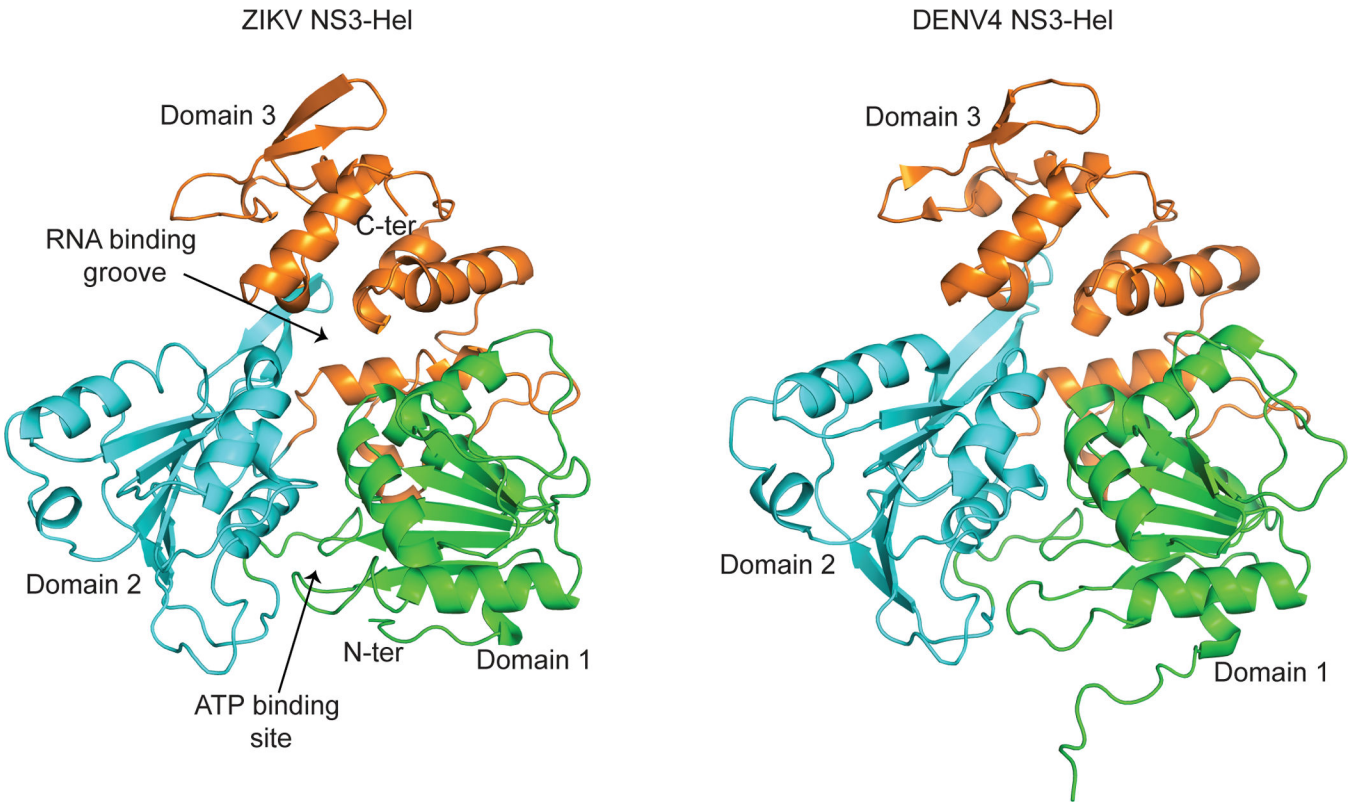

Figure 1.

Structure comparison of ZIKV NS3-Hel with DENV4 NS3 helicase. Overall fold of ZIKV NS3-Hel residues 171:617 (left) and DENV4 helicase[6] (PDB ID 2JLQ, right). RecA like domains 1 and 2 are colored green and cyan, and domain 3 is colored orange. ATP binding pocket and RNA binding groove are indicated.

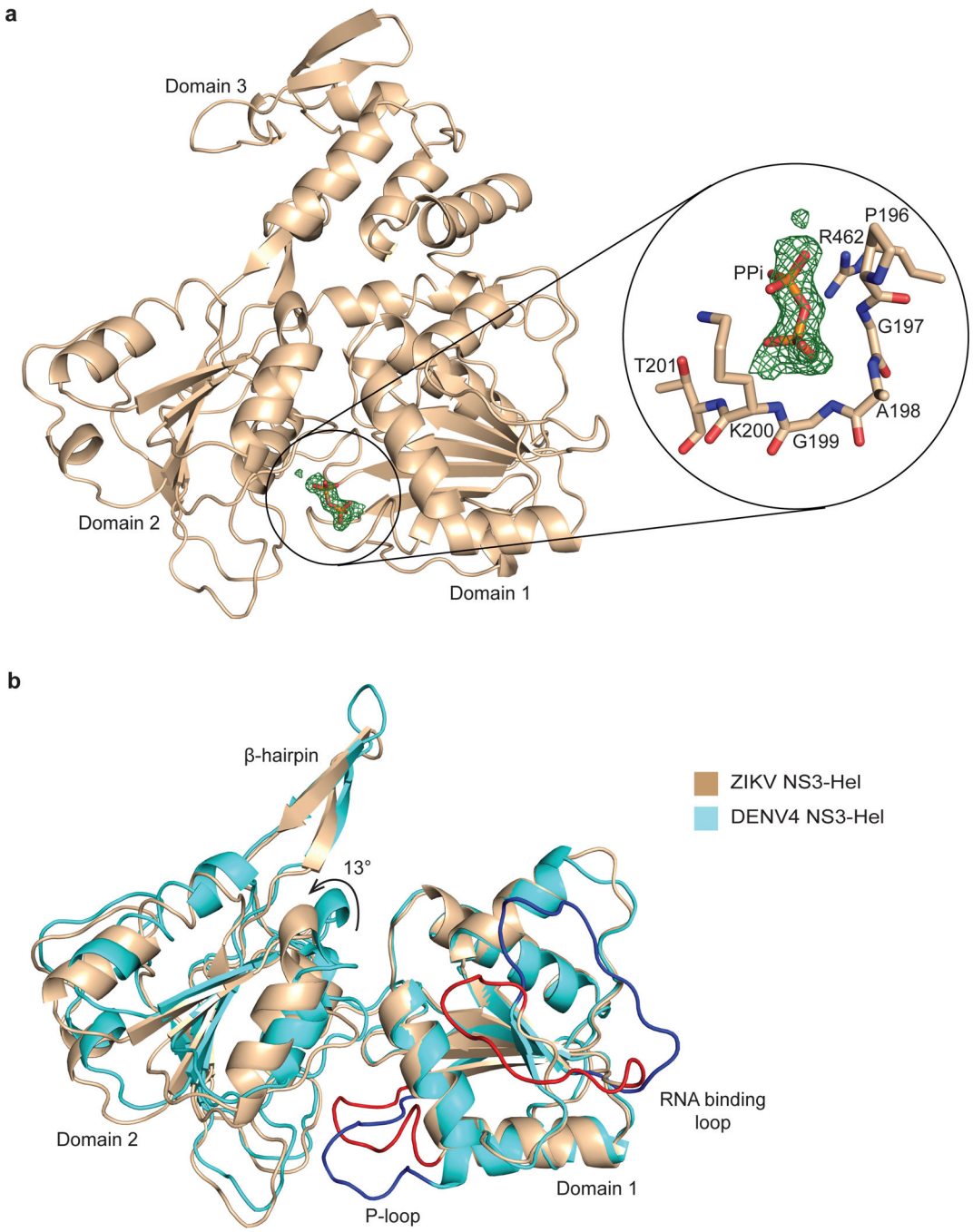

Figure 2.

Features of the ZIKV NS3-Hel structure. (a) Difference electron density (contoured at 3σ) near the P-loop. Magnified view is shown on the right. Residues of the P-loop in the vicinity of the density are shown in tan stick, modeled pyrophosphate (PPi) is shown as orange stick. (b) Superimposition of ZIKV NS3-Hel with DENV4 NS3-Hel via domain 1. Domain 3 has been omitted for clarity. ZIKV NS3-Hel is shown in tan with the P-loop and RNA binding loop in red, and for the DENV4 helicase in cyan and blue respectively.

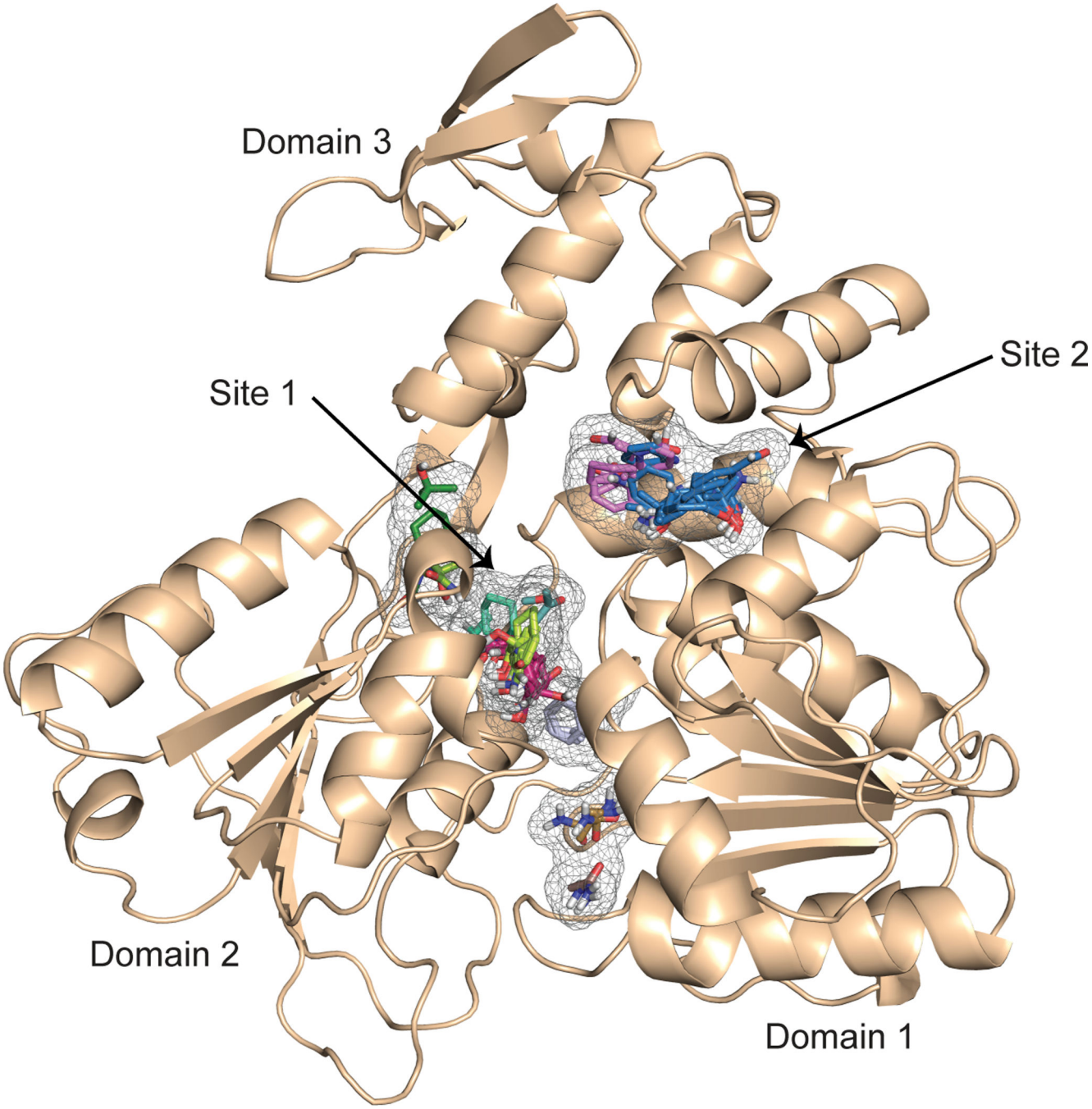

Figure 3.

Hot spots predicted by FTmap for ZIKV NS3-Hel domain. Eleven hot spots predicted by FTmap are shown in grey mesh, and the cluster of probes at each spot shown as sticks of various colors. These hot spots coalesce into two broad and contiguous sites that map between domains 1 and 2 (site 1) and at the confluence of domains 1 and 3 (site 2).